



CERN-EP-2019-016
 LHCb-PAPER-2018-050
 February 18, 2019

arXiv:1902.06794v5 [hep-ex] 14 Aug 2019

Measurement of b -hadron fractions in 13 TeV pp collisions

LHCb collaboration[†]

Abstract

The production fractions of \bar{B}_s^0 and Λ_b^0 hadrons, normalized to the sum of B^- and \bar{B}^0 fractions, are measured in 13 TeV pp collisions using data collected by the LHCb experiment, corresponding to an integrated luminosity of 1.67 fb^{-1} . These ratios, averaged over the b -hadron transverse momenta from 4 to 25 GeV and pseudorapidity from 2 to 5, are 0.122 ± 0.006 for \bar{B}_s^0 , and 0.259 ± 0.018 for Λ_b^0 , where the uncertainties arise from both statistical and systematic sources. The Λ_b^0 ratio depends strongly on transverse momentum, while the \bar{B}_s^0 ratio shows a mild dependence. Neither ratio shows variations with pseudorapidity. The measurements are made using semileptonic decays to minimize theoretical uncertainties. In addition, the ratio of D^+ to D^0 mesons produced in the sum of \bar{B}^0 and B^- semileptonic decays is determined as $0.359 \pm 0.006 \pm 0.009$, where the uncertainties are statistical and systematic.

To be published in Physical Review D Rapid Communications

© 2019 CERN for the benefit of the LHCb collaboration. CC-BY-4.0 licence.

[†]Authors are listed at the end of this paper.

Knowledge of the fragmentation fractions of \bar{B}_s^0 (f_s) and Λ_b^0 ($f_{\Lambda_b^0}$) hadrons is essential for determining absolute branching fractions (\mathcal{B}) of decays of these hadrons at the LHC, allowing measurements, for example, of $\mathcal{B}(\bar{B}_s^0 \rightarrow \mu^+\mu^-)$ [1] and the future evaluation of $|V_{cb}|$ from $\Lambda_b^0 \rightarrow \Lambda_c^+\mu^-\bar{\nu}_\mu$ decays [2].¹ Once these fractions are determined, measurements of absolute branching fractions of B^- and \bar{B}^0 mesons performed at e^+e^- colliders operating at the $\Upsilon(4S)$ resonance can be used to determine the \bar{B}_s^0 and Λ_b^0 branching fractions [3].

In this Letter we measure the ratios $f_s/(f_u + f_d)$ and $f_{\Lambda_b^0}/(f_u + f_d)$, where the denominator is the sum of B^- and \bar{B}^0 contributions, in the LHCb acceptance of pseudorapidity $2 < \eta < 5$ and transverse momentum $4 < p_T < 25$ GeV,² in 13 TeV pp collisions. These ratios can depend on p_T and η ; therefore, we perform the analysis using two-dimensional binning.

Much of the analysis method adopted in this study is an evolution of our previous b -hadron fraction measurements for 7 TeV pp collisions [4]. We use the inclusive semileptonic decays $H_b \rightarrow H_c X \mu^- \bar{\nu}_\mu$, where H_b indicates a b hadron, H_c a charm hadron, and X possible additional particles. Each of the different H_c plus muon final states can originate from the decay of different b hadrons. Semileptonic decays of \bar{B}^0 mesons usually result in a mixture of D^0 and D^+ mesons, while B^- mesons decay predominantly into D^0 mesons with a smaller admixture of D^+ mesons. Both include a tiny component of $D_s^+ \bar{K}$ meson pairs. Similarly, \bar{B}_s^0 mesons decay predominantly into D_s^+ mesons, but can also decay into $D^0 K^+$ and $D^+ K^0$ meson pairs; this is expected if the \bar{B}_s^0 meson decays into an excited D_s^+ state that is heavy enough to decay into a DK pair. We measure this contribution using $D^0 K^+ X \mu^- \bar{\nu}_\mu$ events. Finally, Λ_b^0 baryons decay semileptonically mostly into Λ_c^+ final states, but can also decay into $D^0 p$ and $D^+ n$ pairs. We ignore the contributions of $b \rightarrow u$ decays that comprise approximately 1% of semileptonic b -hadron decays, and contribute almost equally to all b -hadron species. The detailed equations relating these yields to the final results are given in Ref. [4] and in the Supplemental material.

The theoretical basis for this measurement is the near equality of semileptonic widths, Γ_{SL} , for all b -hadron species [5] whose differences are predicted to precisions of about 1%. The values we use for the individual H_b semileptonic branching fractions (\mathcal{B}_{SL}) are listed in Table 1. The H_c decay modes used and their branching fractions are given in Table 2.

The ratio of D^+ to D^0 meson production in the sum of semileptonic \bar{B}^0 and B^- decays, f_+/f_0 , is used to check the analysis method. This result can be related to models of the hadronic final states in B^- and \bar{B}^0 semileptonic decays [6].

The data sample corresponds to 1.67 fb^{-1} of integrated luminosity obtained with the LHCb detector in 13 TeV pp collisions during 2016. The LHCb detector [7, 8] is a single-arm forward spectrometer covering the pseudorapidity range $2 < \eta < 5$, designed for the study of particles containing b or c quarks. The detector elements that are particularly relevant to this analysis are: a silicon-strip vertex detector surrounding the pp interaction region that allows c and b hadrons to be identified from their characteristically long flight distance from the primary vertex (PV); a tracking system that provides a measurement of the momentum, p , of charged particles, two ring-imaging Cherenkov detectors that are able to discriminate between different species of charged hadrons, and a muon detection system.

The online event selection is performed by a trigger [9] which consists of a hardware

¹Mention of a particular decay mode implies the use of the charge-conjugate one as well.

²We use natural units where $c = \hbar = 1$.

Table 1: Branching fractions of semileptonic b -hadron decays from direct measurements for \bar{B}^0 and B^- mesons, ($\langle B \rangle \equiv \langle \bar{B}^0 + B^- \rangle$), and derived for \bar{B}_s^0 and Λ_b^0 hadrons based on the equality of semileptonic widths and the lifetime ratios [3,5]. Corrections to Γ_{SL} for \bar{B}_s^0 ($-1.0 \pm 0.5\%$) and Λ_b^0 ($3.0 \pm 1.5\%$) are applied [5]. Correlations in the \bar{B}^0 and B^- branching fraction measurements have been taken into account. See Ref. [17] for more information.

Particle	τ (ps) measured	\mathcal{B}_{SL} (%) measured	\mathcal{B}_{SL} (%) used
\bar{B}^0	1.520 ± 0.004	10.30 ± 0.19	10.30 ± 0.19
B^-	1.638 ± 0.004	11.08 ± 0.20	11.08 ± 0.20
$\langle B \rangle$		10.70 ± 0.19	10.70 ± 0.19
\bar{B}_s^0	1.526 ± 0.015		10.24 ± 0.21
Λ_b^0	1.470 ± 0.010		10.26 ± 0.25

stage, based on information from the calorimeter and muon systems, followed by a software stage, which applies a full event reconstruction. At the hardware trigger stage, events are required to have a muon with large p_{T} or a hadron, photon or electron with high transverse energy in the calorimeters. For hadrons, the transverse energy threshold is 3.5 GeV. The software trigger requires a two-, three- or four-track secondary vertex with a significant displacement from any primary pp interaction vertex. At least one charged particle must have $p_{\text{T}} > 1.6$ GeV and be inconsistent with originating from a PV. A multivariate algorithm [10] is used for the identification of secondary vertices consistent with the decay of a b hadron.

Simulation is required to model the effects of the detector acceptance and the imposed selection requirements. Here pp collisions are generated using PYTHIA [11] with a specific LHCb configuration [12]. Decays of unstable particles are described by EVTGEN [13], in which final-state radiation is generated using PHOTOS [14]. The interaction of the generated particles with the detector, and its response, are implemented using the GEANT4 toolkit [15] as described in Ref. [16].

Selection criteria are applied to muons and H_c decay particles. The transverse momentum of each hadron must be greater than 0.3 GeV, and that of the muon larger than 1.3 GeV. Each track cannot point to any PV, implemented by requiring $\chi_{\text{IP}}^2 > 9$ with respect to any PV, where χ_{IP}^2 is defined as the difference in the vertex-fit χ^2 of a given PV reconstructed with and without the track under consideration being included. All final

Table 2: Charm-hadron branching fractions for the decay modes used in this analysis. Note, the Λ_c^+ branching fraction has been significantly improved since the previous analysis.

Decay	\mathcal{B} (%)	Source
$D^0 \rightarrow K^- \pi^+$	3.93 ± 0.05	PDG average [3]
$D^+ \rightarrow K^- \pi^+ \pi^+$	9.22 ± 0.17	CLEO-c [18]
$D_s^+ \rightarrow K^- K^+ \pi^+$	5.44 ± 0.18	PDG average [3]
$\Lambda_c^+ \rightarrow p K^- \pi^+$	6.23 ± 0.33	From Refs. [19, 20]

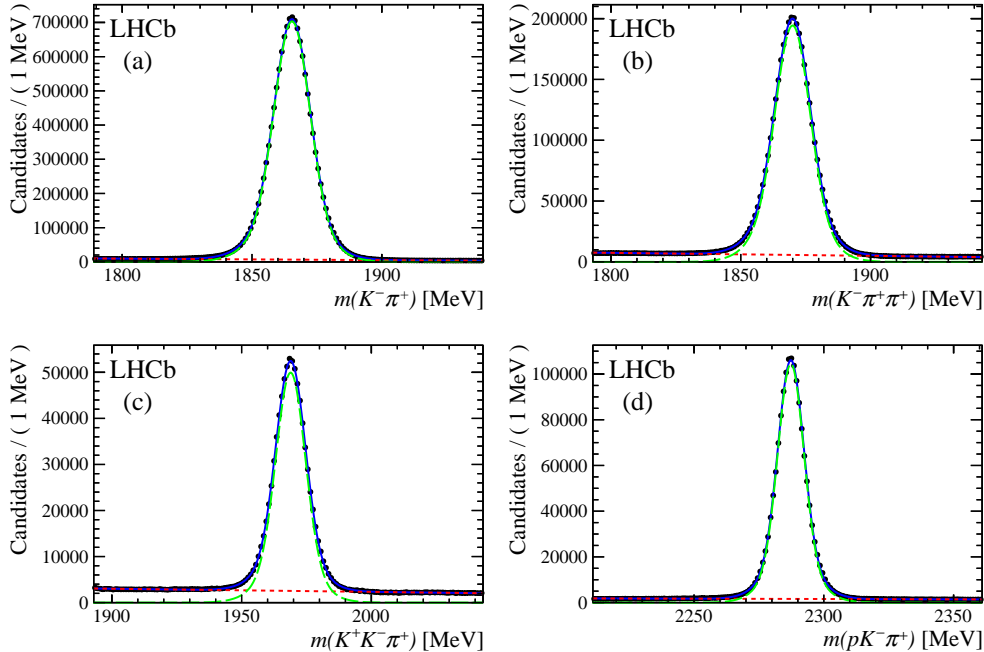


Figure 1: Fit to the mass spectra of the H_c candidates of the selected H_b decays: (a) D^0 , (b) D^+ , (c) D_s^+ mesons, and (d) the Λ_c^+ baryon. The data are shown as black points with error bars. The signal component is shown as the dashed (green) line and the combinatorial background component is shown as the dashed (red) line. The solid (blue) line shows all components added together.

state particles are required to be positively identified using information from the RICH detectors (PID). Particles from H_c decay candidates must have a good fit to a common vertex with $\chi^2/\text{ndof} < 9$, where ndof is the number of degrees of freedom. They must also be well separated from the nearest PV, with the flight distance divided by its uncertainty greater than 5.

Candidate b hadrons are formed by combining H_c and muon candidates originating from a common vertex with $\chi^2/\text{ndof} < 9$ and an $H_c\mu^-$ invariant mass, $m_{H_c\mu^-}$, in the range 3.0–5.0 GeV for D^0 and D^+ , 3.1–5.1 GeV for D_s^+ and 3.3–5.3 GeV for Λ_c^+ candidates. In addition, we define $m_{\text{corr}} \equiv \sqrt{m_{H_c\mu}^2 + p_{\perp}^2} + p_{\perp}$, where p_{\perp} is the magnitude of the combination's momentum component transverse to the b -hadron flight direction; we require that $m_{\text{corr}} > 4.2$ or 4.5 GeV for \bar{B}_s^0 or Λ_b^0 candidates, respectively. For the $D_s^+ \rightarrow K^+K^-\pi^+$ decay mode, vetoes are employed to remove backgrounds from real D^+ or Λ_c^+ decays where the particle assignments are incorrect.

Background from prompt H_c production at the PV needs to be considered. We use the natural logarithm of the H_c impact parameter, IP, with respect to the PV in units of mm. Requiring $\ln(\text{IP}/\text{mm}) > -3$ is found to reduce the prompt component to be below 0.1%, while preserving 97% of all signals. This restriction allows us to perform fits only to the H_c candidate mass spectra to find the b -hadron decay yields.

The H_c candidates mass distributions integrated over $p_T(H_b)$ and η are shown in Fig. 1. They consist of a prominent peak resulting from signal, and a small contribution due to combinatorial background from random combinations of particles that pass the selection. They are fit with a signal component comprised of two Gaussian functions,

and a combinatorial background component modeled as a linear function. The total signal yields for $D^0 X \mu^- \bar{\nu}_\mu$, $D^+ X \mu^- \bar{\nu}_\mu$, $D_s^+ X \mu^- \bar{\nu}_\mu$ and $\Lambda_c^+ \mu^- X \bar{\nu}_\mu$ are 13 775 000, 4 282 700, 845 300, and 1 753 600, respectively.

Background contributions to the b -hadron candidates include hadrons faking muons, false combinations of charm hadrons and muons from the two b hadrons in the event, as well as real muons and charm hadrons from $B \rightarrow D\bar{D}X$ decays, where one of the D mesons decays into a muon. All the backgrounds are evaluated in two-dimensional η and p_T intervals. The first two backgrounds are evaluated using events where the H_c is combined with a muon of the wrong-sign (*e.g.* $D^0 \mu^+$), forbidden in a semileptonic b -hadron decay. The wrong-sign backgrounds are $< 1\%$ for each H_c species. The background from $B \rightarrow D\bar{D}X$ decays is determined by simulating a mixture of these decays using their measured branching fractions [3]. The only decay mode significantly affected is $\bar{B}_s^0 \rightarrow D_s^+ X \mu^- \bar{\nu}_\mu$ with contributions varying from 0.1% for $D^0 D_s^- X$ to 1.8% for $D_s^+ D_s^- X$ due to the large $D_s^+ \rightarrow \mu^+ \nu$ decay rate. The total $B \rightarrow D\bar{D}X$ background is $(5.8 \pm 0.9)\%$.

The dominant component in \bar{B}_s^0 semileptonic decays is $D_s^+ X \mu^- \bar{\nu}_\mu$, where X contains possible additional hadrons. However, the \bar{B}_s^0 meson also can decay into $D^0 K^+$ or $D^+ K^0$ instead of D_s^+ , so we must add this component to the \bar{B}_s^0 rate and subtract it from the $f_u + f_d$ fraction. Similarly, in Λ_b^0 semileptonic decays we find a $D^0 p X$ component. The selection criteria for these final states are similar to those for the $D^0 X \mu^- \bar{\nu}_\mu$ and $\Lambda_c^+ X \mu^- \bar{\nu}_\mu$ final states described above with the addition of a kaon or proton with $p_T > 300$ MeV that has been positively identified. A veto is also applied to reject $D^{*+} \rightarrow \pi^+ D^0$ decays where the pion mimics a kaon or a proton.

These samples contain background, resonant and nonresonant decays. Separation of these components is achieved by using both right-sign (H_c with μ^-) and wrong-sign (H_c with μ^+) candidates. In addition, the logarithm of the difference between the vertex χ^2 formed by the added hadron track and the $D\mu$ system and the vertex χ^2 of the $D\mu$ system, $\ln(\Delta\chi_V^2)$, provides separation between combinatorial background and nonresonant semileptonic decays. True resonant and nonresonant $\bar{B}_s^0 \rightarrow D^0 K^+ \mu^- \bar{\nu}_\mu$ or $\Lambda_b^0 \rightarrow D^0 p \mu^- \bar{\nu}_\mu$ decays peak in the $\ln(\Delta\chi_V^2)$ distribution at a value of unity while the background is smooth and rises at higher values as the added track is generally not associated with the $D^0 \mu^-$ vertex. To distinguish signal from background we define $m(D^0 h)_C \equiv m(D^0 h) - m(D^0) + m(D^0)_{\text{PDG}}$, and perform two-dimensional fits to the $m(D^0 h)_C$ and $\ln(\Delta\chi_V^2)$ distributions, where $h = K^+(p)$ for right-sign \bar{B}_s^0 (Λ_b^0) decays.

The wrong-sign shapes are used to model the backgrounds. The resonant structures are modeled with relativistic Breit–Wigner functions convoluted with Gaussians to take into account the experimental resolution, except for the narrow $D_{s1}(2536)^+$ which is modeled with the sum of two Gaussians with a fixed mean. The nonresonant shape for the $\ln(\Delta\chi_V^2)$ distribution is taken as the same as the resonant one. Figure 2 shows the data and result of the fits for \bar{B}_s^0 and Λ_b^0 candidates.

For the \bar{B}_s^0 case, we find $22\,610 \pm 210$ $D_{s1}(2536)^+$, $14\,290 \pm 260$ $D_{s2}^*(2573)^+$, and $38\,140 \pm 460$ nonresonant decays, confirming the existence of both the D_{s1}^+ [21, 22] and D_{s2}^{*+} [22] particles in semileptonic \bar{B}_s^0 decays with substantially more data, and showing the existence of the nonresonant component. To account for the unmeasured $D^+ K^0$ channel we take different mixtures of D^* and D final states for the different resonant and nonresonant components. The D_{s1}^+ decays dominantly into D^* , while the D_{s2}^{*+} decays dominantly into D mesons [3]. For the nonresonant part we assume equal D^* and D yields.

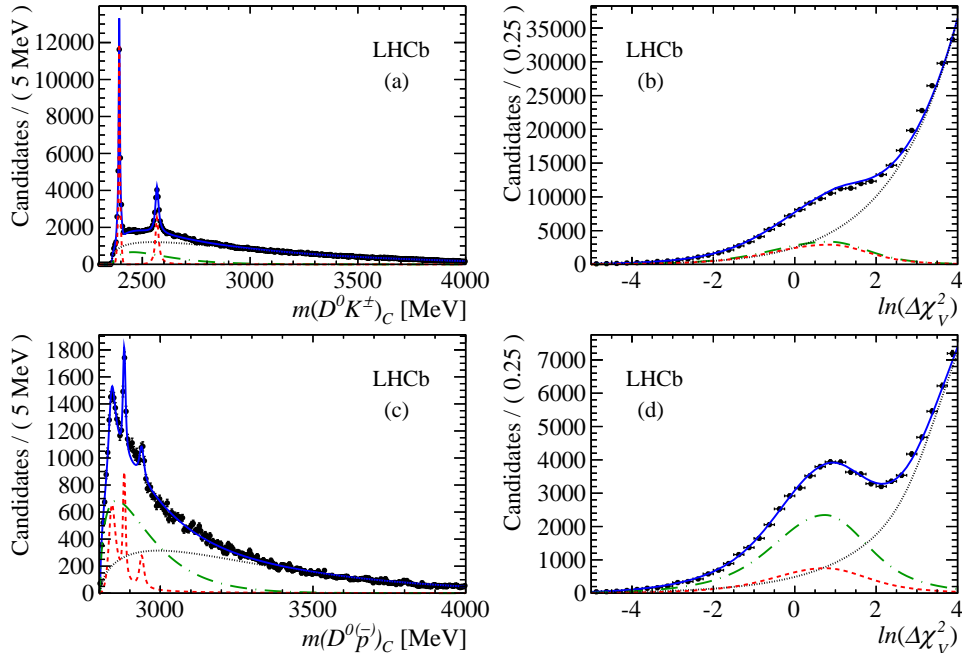


Figure 2: Projections of the two-dimensional fits to the (a) $m(D^0K^\pm)_C$ and (c) $m(D^0\bar{p})_C$ mass distributions and (b, d) $\ln(\Delta\chi^2_V)$ for (top) $D^0K^\pm X\mu^-\bar{\nu}_\mu$ candidates, and (bottom) for $D^0\bar{p} X\mu^-\bar{\nu}_\mu$ candidates. The curves show projections of the 2D fit. The dashed (red) curves show the D_{s1}^+ and D_{s2}^{*+} resonant components in (a) and (b), and $\Lambda_c^+(2860)$, $\Lambda_c^+(2880)$ and $\Lambda_c^+(2940)$ resonant components in (c) and (d). The long-dashed-dotted (green) curves show the nonresonant component, the dotted (black) curves are the background components, whose shapes are determined from wrong-sign combinations, and the solid (blue) curve shows all components added together.

In the Λ_b^0 case, we find 6120 ± 460 $\Lambda_c^+(2860)$, 2200 ± 200 $\Lambda_c^+(2880)$, 1200 ± 260 $\Lambda_c^+(2940)$, and 29770 ± 690 nonresonant events. The decay rate into D^0p is assumed to be equal to that into D^+n using isospin conservation. All decays with an extra hadron have lower detection efficiencies than the sample without.

Efficiencies for all the samples are determined using data in two-dimensional p_T and η bins. Trigger efficiencies are determined using a sample of $B^- \rightarrow J/\psi K^-$, with $J/\psi \rightarrow \mu^+\mu^-$ decays where only one muon track is positively identified, in conjunction with viewing the effects of combinations of different triggers [23]. This sample is also used to determine muon identification efficiencies. Decays of J/ψ mesons to muons reconstructed using partial information from the tracking system, *e.g.* eliminating the vertex locator information, are also used to determine tracking efficiencies using data and to correct the simulation. Finally, the PID efficiencies are evaluated using kaons and pions from $D^{*+} \rightarrow \pi^+ D^0$ decays, with $D^0 \rightarrow K^-\pi^+$, and protons from $\Lambda \rightarrow p\pi^-$ and $\Lambda_c^+ \rightarrow pK^-\pi^+$ decays [24]. In the measurement of b -hadron fraction ratios many of the efficiencies cancel and we are left with only residual effects to which we assign systematic uncertainties.

The b -hadron η and p_T , $p_T(H_b)$, must be known because the b fractions can depend on production kinematics. While η can be evaluated directly using the measured primary and secondary b vertices, the value of $p_T(H_b)$ must be determined to account for the missing neutrino plus extra particles. The correction factor k is given by the ratio of the

average reconstructed to true $p_T(H_b)$ as a function of $m(H_c\mu^-)$ and is determined using simulation. It varies from 0.75 for $m(H_c\mu^-)$ equals 3 GeV to unity at $m(H_c\mu^-) = m(H_b)$.

The distribution of $f_s/(f_u + f_d)$ as a function of $p_T(H_b)$ is shown in Fig. 3. We perform a linear χ^2 fit incorporating a full covariance matrix which takes into account the bin-by-bin correlations introduced from the kaon kinematics, and PID and tracking systematic uncertainties. The factor A in Eq. 1 incorporates the global systematic uncertainties described later, which are independent of $p_T(H_b)$. The resulting function is

$$\frac{f_s}{f_u + f_d}(p_T) = A [p_1 + p_2 \times (p_T - \langle p_T \rangle)], \quad (1)$$

where p_T here refers to $p_T(H_b)$, $A = 1 \pm 0.043$, $p_1 = 0.119 \pm 0.001$, $p_2 = (-0.91 \pm 0.25) \cdot 10^{-3} \text{ GeV}^{-1}$, and $\langle p_T \rangle = 10.1 \text{ GeV}$. The correlation coefficient between the fit parameters is 0.20. After integrating over $p_T(H_b)$, no η dependence is observed (see the Supplemental material).

We determine an average value for $f_s/(f_u + f_d)$ by dividing the yields of \bar{B}_s^0 semileptonic decays by the sum of \bar{B}^0 and B^- semileptonic yields, which are all efficiency-corrected, between the limits of $p_T(H_b)$ of 4 and 25 GeV and η of 2 and 5, resulting in

$$\frac{f_s}{f_u + f_d} = 0.122 \pm 0.006,$$

where the uncertainty contains both statistical and systematic components, with the latter being dominant, and discussed subsequently. The total relative uncertainty is 4.8%.

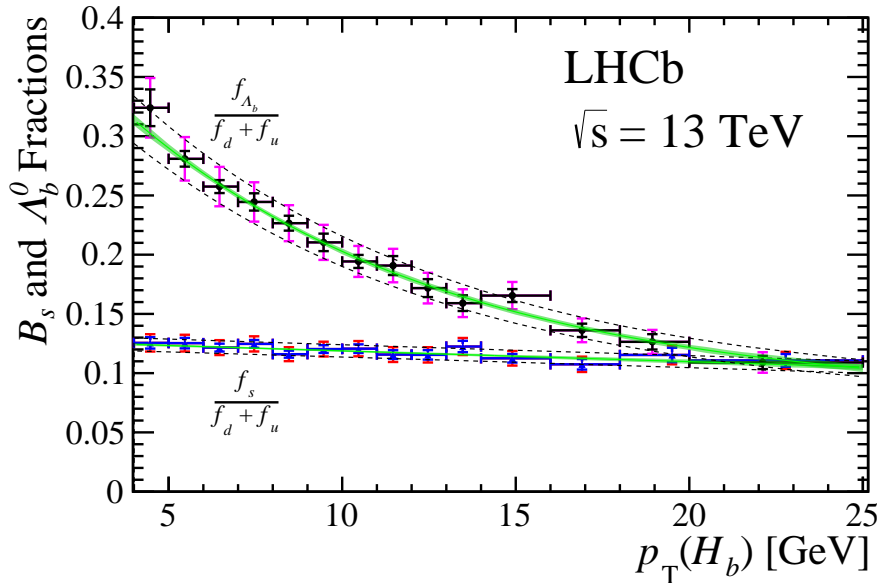


Figure 3: The ratios $f_s/(f_u + f_d)$ and $f_{\Lambda_b^0}/(f_u + f_d)$ in bins of $p_T(H_b)$. The \bar{B}_s^0 data are indicated by solid circles, while the Λ_b^0 by triangles. The smaller (black) error bars show the combined bin-by-bin statistical and systematic uncertainties, and the larger (blue) ones show the global systematics added in quadrature. The fits to the data are shown as the solid (green) bands, whose widths represents the $\pm 1\sigma$ uncertainty limits on the fit shapes, and the dashed (black) lines give the total uncertainty on the fit results including the global scale uncertainty. In the highest two p_T bins the points have been displaced from the center of the bin.

Figure 3 also shows the Λ_b^0 fraction as a function of $p_T(H_b)$ demonstrating a large p_T dependence. The distribution in η is flat. We perform a similar fit as in the \overline{B}_s^0 fraction case, using

$$\frac{f_{\Lambda_b^0}}{f_u + f_d}(p_T) = A [p_1 + \exp(p_2 + p_3 \times p_T)], \quad (2)$$

where p_T here refers to $p_T(H_b)$, $A = 1 \pm 0.061$, $p_1 = (7.93 \pm 1.41) \cdot 10^{-2}$, $p_2 = -1.022 \pm 0.047$, and $p_3 = -0.107 \pm 0.002 \text{ GeV}^{-1}$. The correlation coefficients among the fit parameters are 0.40 (ρ_{12}), -0.95 (ρ_{13}), and -0.63 (ρ_{23}).

The average value for $f_{\Lambda_b^0}/(f_u + f_d)$ is determined using the same method as in the \overline{B}_s^0 case. The result is

$$\frac{f_{\Lambda_b^0}}{f_u + f_d} = 0.259 \pm 0.018,$$

where the dominant uncertainty is systematic, and the statistical uncertainty is included. The overall uncertainty is 6.9%.

As a systematic check of the analysis method, and a useful measurement to test the knowledge of known semileptonic branching fractions and extrapolations used to saturate the unknown portion of the inclusive hadron spectrum, we measure the ratio of the $D^0 X \mu^- \bar{\nu}_\mu$ to $D^+ X \mu^- \bar{\nu}_\mu$ corrected yields f_+/f_0 . We subtract the small contributions from \overline{B}_s^0 and Λ_b^0 decays, and a very small contribution from $B \rightarrow D_s^+ \overline{K} \mu^- X$ decays has been taken into account [25], as in all the fractions measured above.

Assuming f_u equals f_d , Ref. [6] estimates the fraction of $D^+ \mu$ with respect to $D^0 \mu$ modes in the sum of B^- and \overline{B}^0 decays as $0.387 \pm 0.012 \pm 0.026$. The first uncertainty comes from the uncertainties on known measurements. The second uncertainty comes from the different extrapolations from excited D mesons used to saturate the remaining portion of the inclusive rate.

The f_+/f_0 ratio must be independent of η and p_T . To derive an overall value for f_+/f_0 , the $p_T(H_b)$ distribution is fit to a constant. Only the PID and tracking systematic uncertainties on the second pion in the D^+ decay need be considered. Performing a χ^2 fit using the full covariance matrix we find $f_+/f_0 = 0.359 \pm 0.006 \pm 0.009$, where the first uncertainty is from bin-by-bin statistical and systematic uncertainties, including correlations, and the second is systematic. The χ^2/ndof is 0.63, in agreement with a flat spectrum. The measurement is consistent with the prediction and places some constraints on the D^{**} content of semileptonic B decays [6].

The dominant global systematic uncertainties are listed in Table 3. Simulation uncertainties are due to the modeling of excited charm states for the $f_s/(f_u + f_d)$ determination and the weighting required for the $f_{\Lambda_b^0}/(f_u + f_d)$ ratio, due to differences between the simulated and measured p_T spectra. Background uncertainties arise from $D\overline{D}X$ final states with uncertain branching fractions. Cross-feed uncertainties come from errors on efficiency estimates and the assumed D^* to D mixtures. Other smaller uncertainties depend on $p_T(H_b)$ and include tracking (0.2–1.8)%, particle identification (0.4–3.0)%, trigger (0.3–3.9)% and k -factor (0.2–1.8)%.

In conclusion, we measure the ratios of \overline{B}_s^0 and Λ_b^0 production to the sum of B^- and \overline{B}^0 to be $p_T(H_b)$ dependent (see Eqs. 1 and 2). The averages in the ranges $4 < p_T(H_b) < 25 \text{ GeV}$, and $2 < \eta < 5$ are $f_s/(f_u + f_d) = 0.122 \pm 0.006$, and $f_{\Lambda_b^0}/(f_u + f_d) = 0.259 \pm 0.018$, respectively. Using 7 TeV data, LHCb determined $f_s/(f_u + f_d) = 0.1295 \pm 0.0075$ with a $p_T(H_b)$ slope larger than, but consistent with these

Table 3: Global systematic uncertainties. The D^0 and D^+ branching fraction uncertainties are scaled by the fraction of each decay, f_0 and f_+ for $f_s/(f_u + f_d)$ and $f_{\Lambda_b^0}/(f_u + f_d)$ uncertainties.

Source	Value (%)		
	$f_s/(f_u + f_d)$	$f_{\Lambda_b^0}/(f_u + f_d)$	f_+/f_0
Simulation	1.7	2.4	–
Backgrounds	0.9	0.3	–
Cross-feeds	1.2	0.4	0.2
$\mathcal{B}(D^0 \rightarrow K^- \pi^+)$	1.0	1.0	1.3
$\mathcal{B}(D^+ \rightarrow K^+ \pi^- \pi^-)$	0.6	0.6	1.8
$\mathcal{B}(D_s^+ \rightarrow K^+ K^- \pi^+)$	3.3	–	–
$\mathcal{B}(\Lambda_c^+ \rightarrow p K^+ \pi^-)$	–	5.3	–
Measured lifetime ratio	1.2	0.7	–
Γ_{SL} correction	0.5	1.5	–
Total	4.3	6.1	2.2

13 TeV results [26]; no dependence on η was observed. For the Λ_b^0 baryon, the fraction ratio is consistent with the 7 TeV measurements after taking into account the different $p_T(H_b)$ ranges used [4, 27, 28]. We observe no rapidity dependence over a similar $p_T(H_b)$ range as in Ref. [28].

These results are crucial for determining absolute branching fractions of \bar{B}_s^0 and Λ_b^0 hadron decays in LHC experiments. We also determine the ratio of D^0 to D^+ mesons produced in the sum of \bar{B}^0 and B^- semileptonic decays as $f_+/f_0 = 0.359 \pm 0.006 \pm 0.009$.

Acknowledgements

We express our gratitude to our colleagues in the CERN accelerator departments for the excellent performance of the LHC. We thank the technical and administrative staff at the LHCb institutes. We acknowledge support from CERN and from the national agencies: CAPES, CNPq, FAPERJ and FINEP (Brazil); MOST and NSFC (China); CNRS/IN2P3 (France); BMBF, DFG and MPG (Germany); INFN (Italy); NWO (Netherlands); MNiSW and NCN (Poland); MEN/IFA (Romania); MSHE (Russia); MinECo (Spain); SNSF and SER (Switzerland); NASU (Ukraine); STFC (United Kingdom); NSF (USA). We acknowledge the computing resources that are provided by CERN, IN2P3 (France), KIT and DESY (Germany), INFN (Italy), SURF (Netherlands), PIC (Spain), GridPP (United Kingdom), RRCKI and Yandex LLC (Russia), CSCS (Switzerland), IFIN-HH (Romania), CBPF (Brazil), PL-GRID (Poland) and OSC (USA). We are indebted to the communities behind the multiple open-source software packages on which we depend. Individual groups or members have received support from AvH Foundation (Germany); EPLANET, Marie Skłodowska-Curie Actions and ERC (European Union); ANR, Labex P2IO and OCEVU, and Région Auvergne-Rhône-Alpes (France); Key Research Program of Frontier Sciences of CAS, CAS PIFI, and the Thousand Talents Program (China); RFBR, RSF and Yandex LLC (Russia); GVA, XuntaGal and GENCAT (Spain); the Royal Society and the Leverhulme Trust (United Kingdom); Laboratory Directed Research and Development program of LANL (USA).

1 Supplemental material

1.1 Relationships between raw $H_c\mu^-X$ measured yields and corrected yields

The corrected yields for \bar{B}^0 or B^- mesons decaying into $D^0\mu^-\bar{\nu}_\mu X$ or $D^+\mu^-\bar{\nu}_\mu X$, n_{corr} , can be expressed in terms of the measured yields, n , as

$$n_{\text{corr}}(B \rightarrow D^0\mu^-) = \frac{1}{\mathcal{B}(D^0 \rightarrow K^-\pi^+)\epsilon(B \rightarrow D^0)} \times \left[n(D^0\mu^-) - n(D^0K^+\mu^-) \frac{\epsilon(\bar{B}_s^0 \rightarrow D^0)}{\epsilon(\bar{B}_s^0 \rightarrow D^0K^+)} - n(D^0p\mu^-) \frac{\epsilon(\Lambda_b^0 \rightarrow D^0)}{\epsilon(\Lambda_b^0 \rightarrow D^0p)} \right], \quad (3)$$

where we use the shorthand $n(D\mu^-) \equiv n(DX\mu^-\bar{\nu}_\mu)$. An analogous abbreviation ϵ is used for the total trigger and detection efficiencies. For example, the ratio $\epsilon(\bar{B}_s^0 \rightarrow D^0K^+)/\epsilon(\bar{B}_s^0 \rightarrow D^0)$ gives the relative efficiency to reconstruct a charged kaon in semimuonic \bar{B}_s^0 decays producing a D^0 meson. The second term in this equation accounts for the $D^0\mu^-$ pairs originating from a \bar{B}_s^0 decay, such as $\bar{B}_s^0 \rightarrow D^0K^+\mu^-$, while the third term accounts for the $D^0\mu^-$ pairs originating from Λ_b^0 semileptonic decays. These components are determined from the study of the final states $D^0K^+\mu^-$ and $D^0p\mu^-$ respectively. The branching fraction $\mathcal{B}(D^0 \rightarrow K^-\pi^+)$ appears because this decay mode is used in this study. Similarly

$$n_{\text{corr}}(B \rightarrow D^+\mu^-) = \frac{1}{\epsilon(B \rightarrow D^+)} \left[\frac{n(D^+\mu^-)}{\mathcal{B}(D^+ \rightarrow K^-\pi^+\pi^+)} - \frac{n(D^0K^+\mu^-)}{\mathcal{B}(D^0 \rightarrow K^-\pi^+)} \frac{\epsilon(\bar{B}_s^0 \rightarrow D^+)}{\epsilon(\bar{B}_s^0 \rightarrow D^0K^+)} - \frac{n(D^0p\mu^-)}{\mathcal{B}(D^0 \rightarrow K^-\pi^+)} \frac{\epsilon(\Lambda_b^0 \rightarrow D^+)}{\epsilon(\Lambda_b^0 \rightarrow D^0p)} \right]. \quad (4)$$

Both the $D^0X\mu^-\bar{\nu}_\mu$ and the $D^+X\mu^-\bar{\nu}_\mu$ final states contain small components of cross-feed from \bar{B}_s^0 decays to $D^0K^+X\mu^-\bar{\nu}_\mu$ and to $D^+K^0X\mu^-\bar{\nu}_\mu$, and from Λ_b^0 decays to $D^0pX\mu^-\bar{\nu}_\mu$ and to $D^+nX\mu^-\bar{\nu}_\mu$. Here we use isospin symmetry and infer the contributions by $D^+\mu^-$ pairs originating from a \bar{B}_s^0 decay, such as $\bar{B}_s^0 \rightarrow D^+K^0\mu^-\bar{\nu}_\mu$ from the $D^0K^+\mu^-$ final states, and the contributions from $\Lambda_b^0 \rightarrow D^+n\mu^-\bar{\nu}_\mu$ from the $D^0p\mu^-$ yields.

The number of $\bar{B}_s^0 \rightarrow D_s^+X\mu^-\bar{\nu}_\mu$ decays in the final state is given by

$$n_{\text{corr}}(\bar{B}_s^0 \rightarrow D_s^+\mu^-) = \frac{n(D_s^+\mu^-)}{\mathcal{B}(D_s^+ \rightarrow K^+K^-\pi^+)\epsilon(\bar{B}_s^0 \rightarrow D_s^+\mu^-)} - N(\bar{B}^0 + B^-)\mathcal{B}(B \rightarrow D_s^+\bar{K}^0) \frac{\epsilon(\bar{B} \rightarrow D_s^+\bar{K}^0\mu^-)}{\epsilon(\bar{B}_s^0 \rightarrow D_s^+\mu^-)}. \quad (5)$$

In addition, the \bar{B}_s^0 meson decays semileptonically into $DKX\mu^-\bar{\nu}_\mu$, and thus we need to add to Eq. 5 the term

$$n_{\text{corr}}(\bar{B}_s^0 \rightarrow DK\mu^-) = \kappa \frac{n(D^0K^+\mu^-)}{\mathcal{B}(D^0 \rightarrow K^-\pi^+)\epsilon(\bar{B}_s^0 \rightarrow D^0K^+\mu^-)}, \quad (6)$$

where κ accounts for the unmeasured $\bar{B}_s^0 \rightarrow D^+ K X \mu^- \bar{\nu}_\mu$ semileptonic decays. The correction κ is evaluated using the known decay modes of the $D_{s1}(2536)^+$ and $D_{s2}^*(2573)^+$ states and assuming that the nonresonant component of the hadronic mass spectrum decays in equal portions into D or D^* final states. The last term in Eq. 5 accounts for $D_s^+ K X \mu^- \bar{\nu}_\mu$ final states originating from \bar{B}^0 or B^- semileptonic decays, and $N(\bar{B}^0 + B^-)$ indicates the total number of \bar{B}^0 and B^- produced. We derive this correction using the PDG value for the branching fraction $\mathcal{B}(B^- \rightarrow D_s^{(*)+} K^- \mu^- \nu) = (6.1 \pm 1.0) \times 10^{-4}$, and assuming the same rate for \bar{B}_s^0 decays using isospin invariance [3].

The equation for the ratio $f_s/(f_u + f_d)$ is

$$\frac{f_s}{f_u + f_d} = \frac{n_{\text{corr}}(\bar{B}_s^0 \rightarrow D \mu^-)}{n_{\text{corr}}(B \rightarrow D^0 \mu^-) + n_{\text{corr}}(B \rightarrow D^+ \mu^-)} \frac{\tau_{B^-} + \tau_{\bar{B}^0}}{2\tau_{\bar{B}_s^0}} (1 - \xi_s) - \frac{\mathcal{B}(B \rightarrow D_s \bar{K} \mu^-)}{\langle \mathcal{B}_{\text{SL}} \rangle} \frac{\epsilon(\bar{B} \rightarrow D_s^+)}{\epsilon(\bar{B}_s^0 \rightarrow D_s^+)}, \quad (7)$$

where $\bar{B}_s^0 \rightarrow D \mu$ represents \bar{B}_s^0 semileptonic decays to a charmed hadron, given by the sum of the contributions shown in Eqs. 5 and 6, and the symbols τ_{B_i} indicate the B_i hadron lifetimes, that are all well measured [3]. We use the average \bar{B}_s^0 lifetime, 1.526 ± 0.015 ps. This equation assumes equality of the semileptonic widths of all the b -hadron species. This is a reliable assumption, as corrections in HQET arise only to order $1/m_b^2$ and the SU(3) breaking correction is quite small, $(-1.0 \pm 0.5)\%$ [5]. The parameter ξ_s accounts for this small adjustment. The second term is the subtraction of the $B^- \rightarrow D_s^+ \bar{K} X \mu^- \bar{\nu}_\mu$ component that is reconstructed in the signal sample as described in Eq. 5. The \mathcal{B}_{SL} term in the denominator is the semileptonic branching fraction of the \bar{B}_s^0 derived using the equality of the semileptonic widths and the measured lifetime of the \bar{B}_s^0 , listed in Table 1.

The Λ_b^0 corrected yield is derived in an analogous manner

$$n_{\text{corr}}(\Lambda_b^0 \rightarrow H_c \mu^-) = \frac{n(\Lambda_c^+ \mu^-)}{\mathcal{B}(\Lambda_c^+ \rightarrow p K^- \pi^+) \epsilon(\Lambda_b^0 \rightarrow \Lambda_c^+)} + 2 \frac{n(D^0 p \mu^-)}{\mathcal{B}(D^0 \rightarrow K^- \pi^+) \epsilon(\Lambda_b^0 \rightarrow D^0 p)}, \quad (8)$$

where H_c represents a generic charmed hadron. The second term includes the cross-feed channel and the factor of two accounts for the isospin $\Lambda_b^0 \rightarrow D^+ n \mu^-$ decay. The Λ_b^0 fraction is written as

$$\frac{f_{\Lambda_b^0}}{f_u + f_d} = \frac{n_{\text{corr}}(\Lambda_b^0 \rightarrow H_c \mu^-)}{n_{\text{corr}}(B \rightarrow D^0 \mu^-) + n_{\text{corr}}(B \rightarrow D^+ \mu^-)} \frac{\tau_{B^-} + \tau_{\bar{B}^0}}{2\tau_{\Lambda_b^0}} (1 - \xi_{\Lambda_b^0}). \quad (9)$$

While we assume near equality of the semileptonic widths of different b hadrons, we apply a small adjustment $\xi_{\Lambda_b^0} = (3.0 \pm 1.5)\%$, to account for the chromomagnetic correction, affecting b -flavored mesons but not b baryons [5]. The uncertainty is evaluated with conservative assumptions for all the parameters of the heavy quark expansion.

1.2 Table of b -fractions versus $p_T(H_b)$

Table 4: Values of $f_s/(f_u + f_d)$ and $f_{\Lambda_b^0}/(f_u + f_d)$ in each $p_T(H_b)$ bin. The first uncertainty is statistical and incorporates both the uncertainties due to the data sample size and the finite amount of simulated events, while the second is the overall systematic uncertainty, including global and bin-dependent systematic uncertainties.

$p_T(H_b)$ [GeV]	$f_s/(f_u + f_d)$	$f_{\Lambda_b^0}/(f_u + f_d)$
4–5	$0.125 \pm 0.001 \pm 0.007$	$0.324 \pm 0.001 \pm 0.025$
5–6	$0.125 \pm 0.001 \pm 0.007$	$0.281 \pm 0.001 \pm 0.018$
6–7	$0.122 \pm 0.001 \pm 0.006$	$0.257 \pm 0.001 \pm 0.017$
7–8	$0.125 \pm 0.001 \pm 0.006$	$0.245 \pm 0.001 \pm 0.017$
8–9	$0.116 \pm 0.001 \pm 0.006$	$0.227 \pm 0.001 \pm 0.015$
9–10	$0.120 \pm 0.001 \pm 0.006$	$0.210 \pm 0.001 \pm 0.015$
10–11	$0.121 \pm 0.001 \pm 0.006$	$0.194 \pm 0.001 \pm 0.013$
11–12	$0.116 \pm 0.001 \pm 0.006$	$0.191 \pm 0.001 \pm 0.014$
12–13	$0.116 \pm 0.001 \pm 0.006$	$0.172 \pm 0.001 \pm 0.013$
13–14	$0.122 \pm 0.001 \pm 0.007$	$0.159 \pm 0.001 \pm 0.012$
14–16	$0.112 \pm 0.001 \pm 0.006$	$0.165 \pm 0.001 \pm 0.012$
16–18	$0.107 \pm 0.001 \pm 0.006$	$0.136 \pm 0.001 \pm 0.010$
18–20	$0.115 \pm 0.001 \pm 0.008$	$0.126 \pm 0.001 \pm 0.010$
20–25	$0.111 \pm 0.001 \pm 0.007$	$0.109 \pm 0.001 \pm 0.009$

1.3 Fraction ratios as functions of η

Figure 4 shows measurements of the fraction ratios $f_s/(f_u + f_d)$ and $f_{\Lambda_b^0}/(f_u + f_d)$ as functions of η , integrated over p_T . No η dependence is visible with the current data sample.

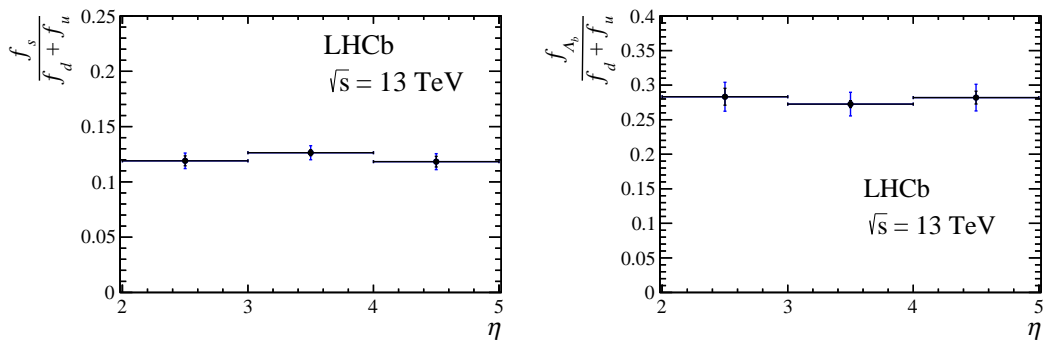


Figure 4: Measurement of the fraction ratios (a) $f_s/(f_u + f_d)$ and (b) $f_{\Lambda_b^0}/(f_u + f_d)$ as functions of η integrated over p_T .

1.4 Correlation matrices for the fits to $f_s/(f_u + f_d)$ and $f_{\Lambda_b^0}/(f_u + f_d)$

Table 5 shows the covariance matrix among the different $p_T(H_b)$ bins for $f_s/(f_u + f_d)$, while Table 6 shows the covariance matrix among the different $p_T(H_b)$ bins for $f_{\Lambda_b^0}/(f_u + f_d)$.

Table 5: Covariance matrix for $f_s/(f_u + f_d)$ in $p_T(H_b)$ [GeV] bins; it accounts for statistical and bin-dependent systematic uncertainties, but not the global systematic uncertainties.

$p_T(H_b)$	4-5	5-6	6-7	7-8	8-9	9-10	10-11	11-12	12-13	13-14	14-16	16-18	18-20	20-25
4-5	2.30E-05	3.80E-06	1.84E-06	1.53E-06	9.28E-07	1.54E-06	1.77E-06	9.05E-07	7.47E-07	6.99E-07	6.46E-07	6.84E-07	5.47E-07	5.55E-07
5-6	3.80E-06	1.96E-05	2.37E-06	2.02E-06	1.23E-06	2.05E-06	2.36E-06	1.22E-06	1.04E-06	9.64E-07	8.94E-07	9.85E-07	8.04E-07	8.00E-07
6-7	1.84E-06	2.37E-06	1.10E-05	1.08E-06	6.71E-07	1.14E-06	1.32E-06	6.94E-07	5.83E-07	5.46E-07	5.18E-07	5.60E-07	4.67E-07	4.89E-07
7-8	1.53E-06	2.02E-06	1.08E-06	1.08E-06	6.46E-07	1.10E-06	1.27E-06	6.75E-07	5.73E-07	5.43E-07	5.06E-07	5.48E-07	4.80E-07	4.86E-07
8-9	9.28E-07	1.23E-06	6.71E-07	6.46E-07	8.73E-06	7.75E-07	9.09E-07	5.07E-07	4.26E-07	4.04E-07	3.79E-07	4.16E-07	3.77E-07	3.88E-07
9-10	1.54E-06	2.05E-06	1.14E-06	1.10E-06	7.75E-07	1.09E-05	1.66E-06	9.39E-07	8.03E-07	7.62E-07	7.24E-07	7.77E-07	7.01E-07	7.34E-07
10-11	1.77E-06	2.36E-06	1.32E-06	1.27E-06	9.09E-07	1.66E-06	1.33E-05	1.13E-06	9.90E-07	9.33E-07	9.37E-07	1.00E-06	9.03E-07	9.58E-07
11-12	9.05E-07	1.22E-06	6.94E-07	6.75E-07	5.07E-07	9.39E-07	1.13E-06	1.33E-05	5.94E-07	5.64E-07	5.74E-07	6.24E-07	5.73E-07	6.17E-07
12-13	7.47E-07	1.04E-06	5.83E-07	5.73E-07	4.26E-07	8.03E-07	9.90E-07	5.94E-07	1.60E-05	5.42E-07	5.62E-07	6.33E-07	5.73E-07	6.08E-07
13-14	6.99E-07	9.64E-07	5.46E-07	5.43E-07	4.04E-07	7.62E-07	9.33E-07	5.64E-07	5.42E-07	2.31E-05	5.31E-07	6.33E-07	5.98E-07	6.13E-07
14-16	6.46E-07	8.94E-07	5.18E-07	5.06E-07	3.79E-07	7.24E-07	9.37E-07	5.74E-07	5.62E-07	5.31E-07	1.32E-05	7.11E-07	6.66E-07	7.27E-07
16-18	6.84E-07	9.85E-07	5.60E-07	5.48E-07	4.16E-07	7.77E-07	1.00E-06	6.24E-07	6.33E-07	6.33E-07	7.11E-07	1.96E-05	8.08E-07	9.33E-07
18-20	5.47E-07	8.04E-07	4.67E-07	4.80E-07	3.77E-07	7.01E-07	9.03E-07	5.73E-07	5.98E-07	5.98E-07	6.66E-07	8.08E-07	3.71E-05	9.58E-07
20-25	5.55E-07	8.00E-07	4.89E-07	4.86E-07	3.88E-07	7.34E-07	9.58E-07	6.17E-07	6.08E-07	6.13E-07	7.27E-07	9.33E-07	9.58E-07	2.93E-05

Table 6: Covariance matrix for $f_{\Lambda_b^0}/(f_u + f_d)$ in $p_T(H_b)$ [GeV] bins; it accounts for statistical and bin-dependent systematic uncertainties, but not the global systematic uncertainties.

$p_T(H_b)$	4-5	5-6	6-7	7-8	8-9	9-10	10-11	11-12	12-13	13-14	14-16	16-18	18-20	20-25
4-5	2.40E-4	3.21E-5	2.08E-5	5.03E-5	3.36E-5	4.21E-5	1.60E-5	3.50E-5	2.47E-5	1.30E-5	6.20E-6	3.10E-6	2.60E-6	3.46E-6
5-6	3.21E-5	4.34E-5	5.05E-6	1.30E-5	8.90E-6	1.12E-5	4.47E-6	9.65E-6	7.12E-6	3.73E-6	1.80E-6	9.11E-7	7.82E-7	1.12E-6
6-7	2.08E-5	5.05E-6	2.99E-5	9.39E-6	6.55E-6	8.41E-6	3.35E-6	7.43E-6	5.44E-6	2.86E-6	1.43E-6	7.04E-7	6.25E-7	8.96E-7
7-8	5.03E-5	1.30E-5	9.39E-6	5.32E-5	1.97E-5	2.56E-5	1.05E-5	2.26E-5	1.72E-5	9.14E-6	4.53E-6	2.33E-6	2.04E-6	3.01E-6
8-9	3.36E-5	8.90E-6	6.55E-6	1.97E-5	3.96E-5	2.10E-5	8.88E-6	1.95E-5	1.47E-5	7.91E-6	3.91E-6	2.03E-6	1.75E-6	2.75E-6
9-10	4.21E-5	1.12E-5	8.41E-6	2.56E-5	2.10E-5	5.44E-5	1.27E-5	2.81E-5	2.14E-5	1.21E-5	5.88E-6	3.11E-6	2.69E-6	4.44E-6
10-11	1.60E-5	4.47E-6	3.35E-6	1.05E-5	8.88E-6	1.27E-5	3.03E-5	1.33E-5	1.10E-5	6.15E-6	3.07E-6	1.67E-6	1.43E-6	2.48E-6
11-12	3.50E-5	9.65E-6	7.43E-6	2.26E-5	1.95E-5	2.81E-5	1.33E-5	6.41E-5	2.54E-5	1.42E-5	7.23E-6	3.98E-6	3.44E-6	5.86E-6
12-13	2.47E-5	7.12E-6	5.44E-6	1.72E-5	1.47E-5	2.14E-5	1.10E-5	2.54E-5	5.71E-5	1.36E-5	6.78E-6	3.85E-6	3.41E-6	6.10E-6
13-14	1.30E-5	3.73E-6	2.86E-6	9.14E-6	7.90E-6	1.21E-5	6.15E-6	1.42E-5	1.36E-5	4.37E-5	4.23E-6	2.47E-6	7.22E-6	3.88E-6
14-16	6.20E-6	1.80E-6	1.43E-6	4.53E-6	3.91E-6	5.88E-6	3.07E-6	7.23E-6	6.78E-6	4.23E-6	3.01E-5	1.35E-6	1.21E-6	2.24E-6
16-18	3.10E-6	9.11E-7	7.04E-7	2.33E-6	2.03E-6	3.11E-6	1.67E-6	3.98E-6	3.85E-6	2.47E-6	1.35E-6	3.17E-5	8.03E-7	1.54E-6
18-20	2.61E-6	7.82E-7	6.25E-7	2.04E-6	1.75E-6	2.67E-6	1.43E-6	3.44E-6	3.41E-6	2.22E-6	1.21E-6	8.03E-7	4.21E-5	1.62E-6
20-25	3.46E-6	1.12E-6	8.97E-7	3.01E-6	2.75E-6	4.44E-6	2.48E-6	5.83E-6	6.10E-6	3.88E-6	2.24E-6	1.54E-6	1.62E-6	3.09E-5

References

- [1] CMS collaboration, V. Khachatryan *et al.*, *Observation of the rare $B_s^0 \rightarrow \mu^+\mu^-$ decay from the combined analysis of CMS and LHCb data*, Nature **522** (2015) 68, [arXiv:1411.4413](#).
- [2] LHCb collaboration, R. Aaij *et al.*, *Measurement of the shape of the $\Lambda_b^0 \rightarrow \Lambda_c^+\mu^-\bar{\nu}_\mu$ differential decay rate*, Phys. Rev. **D96** (2017) 112005, [arXiv:1709.01920](#).
- [3] Particle Data Group, M. Tanabashi *et al.*, *Review of Particle Physics*, Phys. Rev. **D98** (2018) 030001.
- [4] LHCb collaboration, R. Aaij *et al.*, *Measurement of b hadron production fractions in 7 TeV pp collisions*, Phys. Rev. **D85** (2012) 032008, [arXiv:1111.2357](#).
- [5] I. I. Bigi, T. Mannel, and N. Uraltsev, *Semileptonic width ratios among beauty hadrons*, JHEP **09** (2011) 012, [arXiv:1105.4574](#).
- [6] M. Rudolph, *An experimentalists guide to the semileptonic bottom to charm branching fractions*, Int. J. Mod. Phys. **A33** (2018) 1850176, [arXiv:1805.05659](#).
- [7] LHCb collaboration, A. A. Alves Jr. *et al.*, *The LHCb detector at the LHC*, JINST **3** (2008) S08005.
- [8] LHCb collaboration, R. Aaij *et al.*, *LHCb detector performance*, Int. J. Mod. Phys. **A30** (2015) 1530022, [arXiv:1412.6352](#).
- [9] R. Aaij *et al.*, *The LHCb trigger and its performance in 2011*, JINST **8** (2013) P04022, [arXiv:1211.3055](#).
- [10] V. V. Gligorov and M. Williams, *Efficient, reliable and fast high-level triggering using a bonsai boosted decision tree*, JINST **8** (2013) P02013, [arXiv:1210.6861](#).
- [11] T. Sjöstrand, S. Mrenna, and P. Skands, *A brief introduction to PYTHIA 8.1*, Comput. Phys. Commun. **178** (2008) 852, [arXiv:0710.3820](#); T. Sjöstrand, S. Mrenna, and P. Skands, *PYTHIA 6.4 physics and manual*, JHEP **05** (2006) 026, [arXiv:hep-ph/0603175](#).
- [12] I. Belyaev *et al.*, *Handling of the generation of primary events in Gauss, the LHCb simulation framework*, J. Phys. Conf. Ser. **331** (2011) 032047.
- [13] D. J. Lange, *The EvtGen particle decay simulation package*, Nucl. Instrum. Meth. **A462** (2001) 152.
- [14] P. Golonka and Z. Was, *PHOTOS Monte Carlo: A precision tool for QED corrections in Z and W decays*, Eur. Phys. J. **C45** (2006) 97, [arXiv:hep-ph/0506026](#).
- [15] Geant4 collaboration, J. Allison *et al.*, *Geant4 developments and applications*, IEEE Trans. Nucl. Sci. **53** (2006) 270; Geant4 collaboration, S. Agostinelli *et al.*, *Geant4: A simulation toolkit*, Nucl. Instrum. Meth. **A506** (2003) 250.

- [16] M. Clemencic *et al.*, *The LHCb simulation application, Gauss: Design, evolution and experience*, J. Phys. Conf. Ser. **331** (2011) 032023.
- [17] LHCb collaboration, R. Aaij *et al.*, *Measurement of the b -quark production cross-section in 7 and 13 TeV pp collisions*, Phys. Rev. Lett. **118** (2017) 052002, Erratum *ibid.* **119** (2017) 169901, [arXiv:1612.05140](#).
- [18] CLEO collaboration, G. Bonvicini *et al.*, *Updated measurements of absolute D^+ and D^0 hadronic branching fractions and $\sigma(e^+e^- \rightarrow D\bar{D})$ at $E_{\text{cm}} = 3774$ MeV*, Phys. Rev. **D89** (2014) 072002, Erratum *ibid.* **D91** (2015) 019903, [arXiv:1312.6775](#).
- [19] BESIII collaboration, M. Ablikim *et al.*, *Measurements of absolute hadronic branching fractions of the Λ_c^+ baryon*, Phys. Rev. Lett. **116** (2016) 052001, [arXiv:1511.08380](#).
- [20] Belle collaboration, A. Zupanc *et al.*, *Measurement of the branching fraction $\mathcal{B}(\Lambda_c^+ \rightarrow pK^-\pi^+)$* , Phys. Rev. Lett. **113** (2014) 042002, [arXiv:1312.7826](#).
- [21] D0 collaboration, V. M. Abazov *et al.*, *Measurement of the B_s^0 semileptonic branching ratio to an orbitally excited D_s^{**} state: $\mathcal{B}(B_s^0 \rightarrow D_{s1}^-(2536)\mu^+\nu X)$* , Phys. Rev. Lett. **102** (2009) 051801, [arXiv:0712.3789](#).
- [22] LHCb collaboration, R. Aaij *et al.*, *First observation of $\bar{B}_s^0 \rightarrow D_{s2}^{*+} X \mu^- \bar{\nu}$ decays*, Phys. Lett. **B698** (2011) 14, [arXiv:1102.0348](#).
- [23] S. Tolk, J. Albrecht, F. Dettori, and A. Pellegrino, *Data driven trigger efficiency determination at LHCb*, CERN-LHCb-PUB-2014-039, LHCb-PUB-2014-039.
- [24] R. Aaij *et al.*, *Selection and processing of calibration samples to measure the particle identification performance of the LHCb experiment in Run 2*, [arXiv:1803.00824](#).
- [25] BaBar collaboration, P. del Amo Sanchez *et al.*, *Observation of the decay $B^- \rightarrow D_s^{(*)+} K^- \ell^- \bar{\nu}_\ell$* , Phys. Rev. Lett. **107** (2011) 041804, [arXiv:1012.4158](#).
- [26] LHCb collaboration, R. Aaij *et al.*, *Measurement of the fragmentation fraction ratio f_s/f_d and its dependence on B meson kinematics*, JHEP **04** (2013) 001, f_s/f_d value updated in LHCb-CONF-2013-011.
- [27] LHCb collaboration, R. Aaij *et al.*, *Study of the kinematic dependences of Λ_b^0 production in pp collisions and a measurement of the $\Lambda_b^0 \rightarrow \Lambda_c^+ \pi^-$ branching fraction*, JHEP **08** (2014) 143, [arXiv:1405.6842](#).
- [28] LHCb collaboration, R. Aaij *et al.*, *Study of the production of Λ_b^0 and \bar{B}^0 hadrons in pp collisions and first measurement of the $\Lambda_b^0 \rightarrow J/\psi p K^-$ branching fraction*, Chin. Phys. **C40** (2016) 011001, [arXiv:1509.00292](#).

LHCb Collaboration

R. Aaij²⁹, C. Abellán Beteta⁴⁶, B. Adeva⁴³, M. Adinolfi⁵⁰, C.A. Aidala⁷⁷, Z. Ajaltouni⁷, S. Akar⁶¹, P. Albicocco²⁰, J. Albrecht¹², F. Alessio⁴⁴, M. Alexander⁵⁵, A. Alfonso Alberio⁴², G. Alkhazov³⁵, P. Alvarez Cartelle⁵⁷, A.A. Alves Jr⁴³, S. Amato², S. Amerio²⁵, Y. Amhis⁹, L. An¹⁹, L. Anderlini¹⁹, G. Andreassi⁴⁵, M. Andreotti¹⁸, J.E. Andrews⁶², F. Archilli²⁹, J. Arnau Romeu⁸, A. Artamonov⁴¹, M. Artuso⁶³, K. Arzymatov³⁹, E. Aslanides⁸, M. Atzeni⁴⁶, B. Audurier²⁴, S. Bachmann¹⁴, J.J. Back⁵², S. Baker⁵⁷, V. Balagura^{9,b}, W. Baldini¹⁸, A. Baranov³⁹, R.J. Barlow⁵⁸, G.C. Barrand⁹, S. Barsuk⁹, W. Barter⁵⁷, M. Bartolini²¹, F. Baryshnikov⁷³, V. Batozskaya³³, B. Batsukh⁶³, A. Battig¹², V. Battista⁴⁵, A. Bay⁴⁵, J. Beddow⁵⁵, F. Bedeschi²⁶, I. Bediaga¹, A. Beiter⁶³, L.J. Bel²⁹, S. Belin²⁴, N. Belyi⁴, V. Bellee⁴⁵, N. Belloli^{22,i}, K. Belous⁴¹, I. Belyaev³⁶, G. Bencivenni²⁰, E. Ben-Haim¹⁰, S. Benson²⁹, S. Beranek¹¹, A. Berezhnoy³⁷, R. Bernet⁴⁶, D. Berninghoff¹⁴, E. Bertholet¹⁰, A. Bertolin²⁵, C. Betancourt⁴⁶, F. Betti^{17,44}, M.O. Bettler⁵¹, Ia. Bezshyiko⁴⁶, S. Bhasin⁵⁰, J. Bhom³¹, M.S. Bieker¹², S. Bifani⁴⁹, P. Billoir¹⁰, A. Birnkraut¹², A. Bizzeti^{19,u}, M. Björn⁵⁹, M.P. Blago⁴⁴, T. Blake⁵², F. Blanc⁴⁵, S. Blusk⁶³, D. Bobulska⁵⁵, V. Bocci²⁸, O. Boente Garcia⁴³, T. Boettcher⁶⁰, A. Bondar^{40,x}, N. Bondar³⁵, S. Borghi^{58,44}, M. Borisyak³⁹, M. Borsato¹⁴, M. Boubdir¹¹, T.J.V. Bowcock⁵⁶, C. Bozzi^{18,44}, S. Braun¹⁴, M. Brodski⁴⁴, J. Brodzicka³¹, A. Brossa Gonzalo⁵², D. Brundu^{24,44}, E. Buchanan⁵⁰, A. Buonauro⁴⁶, C. Buri⁵⁸, A. Bursche²⁴, J. Buytaert⁴⁴, W. Byczynski⁴⁴, S. Cadeddu²⁴, H. Cai⁶⁷, R. Calabrese^{18,g}, R. Calladine⁴⁹, M. Calvi^{22,i}, M. Calvo Gomez^{42,m}, A. Camboni^{42,m}, P. Campana²⁰, D.H. Campora Perez⁴⁴, L. Capriotti^{17,e}, A. Carbone^{17,e}, G. Carboni²⁷, R. Cardinale²¹, A. Cardini²⁴, P. Carniti^{22,i}, K. Carvalho Akiba², G. Casse⁵⁶, M. Cattaneo⁴⁴, G. Cavallero²¹, R. Cenci^{26,p}, D. Chamont⁹, M.G. Chapman⁵⁰, M. Charles¹⁰, Ph. Charpentier⁴⁴, G. Chatzikonstantinidis⁴⁹, M. Chefdeville⁶, V. Chekalina³⁹, C. Chen³, S. Chen²⁴, S.-G. Chitic⁴⁴, V. Chobanova⁴³, M. Chrzasczcz⁴⁴, A. Chubykin³⁵, P. Ciambrone²⁰, X. Cid Vidal⁴³, G. Ciezarek⁴⁴, F. Cindolo¹⁷, P.E.L. Clarke⁵⁴, M. Clemencic⁴⁴, H.V. Cliff⁵¹, J. Closier⁴⁴, V. Coco⁴⁴, J.A.B. Coelho⁹, J. Cogan⁸, E. Cogneras⁷, L. Cojocariu³⁴, P. Collins⁴⁴, T. Colombo⁴⁴, A. Comerma-Montells¹⁴, A. Contu²⁴, G. Coombs⁴⁴, S. Coquereau⁴², G. Corti⁴⁴, M. Corvo^{18,g}, C.M. Costa Sobral⁵², B. Couturier⁴⁴, G.A. Cowan⁵⁴, D.C. Craik⁶⁰, A. Crocombe⁵², M. Cruz Torres¹, R. Currie⁵⁴, F. Da Cunha Marinho², C.L. Da Silva⁷⁸, E. Dall'Occo²⁹, J. Dalseno^{43,v}, C. D'Ambrosio⁴⁴, A. Danilina³⁶, P. d'Argent¹⁴, A. Davis⁵⁸, O. De Aguiar Francisco⁴⁴, K. De Bruyn⁴⁴, S. De Capua⁵⁸, M. De Cian⁴⁵, J.M. De Miranda¹, L. De Paula², M. De Serio^{16,d}, P. De Simone²⁰, J.A. de Vries²⁹, C.T. Dean⁵⁵, W. Dean⁷⁷, D. Decamp⁶, L. Del Buono¹⁰, B. Delaney⁵¹, H.-P. Dembinski¹³, M. Demmer¹², A. Dendek³², D. Derkach⁷⁴, O. Deschamps⁷, F. Desse⁹, F. Dettori⁵⁶, B. Dey⁶⁸, A. Di Canto⁴⁴, P. Di Nezza²⁰, S. Didenko⁷³, H. Dijkstra⁴⁴, F. Dordei²⁴, M. Dorigo^{44,y}, A.C. dos Reis¹, A. Dosil Suárez⁴³, L. Douglas⁵⁵, A. Dovbnya⁴⁷, K. Dreimanis⁵⁶, L. Dufour²⁹, G. Dujany¹⁰, P. Durante⁴⁴, J.M. Durham⁷⁸, D. Dutta⁵⁸, R. Dzhelyadin^{41,†}, M. Dziewiecki¹⁴, A. Dziurda³¹, A. Dzyuba³⁵, S. Easo⁵³, U. Egede⁵⁷, V. Egorychev³⁶, S. Eidelman^{40,x}, S. Eisenhardt⁵⁴, U. Eitschberger¹², R. Ekelhof¹², L. Eklund⁵⁵, S. Ely⁶³, A. Ene³⁴, S. Escher¹¹, S. Esen²⁹, T. Evans⁶¹, A. Falabella¹⁷, C. Färber⁴⁴, N. Farley⁴⁹, S. Farry⁵⁶, D. Fazzini^{22,44,i}, M. Féo⁴⁴, P. Fernandez Declara⁴⁴, A. Fernandez Prieto⁴³, F. Ferrari^{17,e}, L. Ferreira Lopes⁴⁵, F. Ferreira Rodrigues², M. Ferro-Luzzi⁴⁴, S. Filippov³⁸, R.A. Fini¹⁶, M. Fiorini^{18,g}, M. Firlej³², C. Fitzpatrick⁴⁵, T. Fiutowski³², F. Fleuret^{9,b}, M. Fontana⁴⁴, F. Fontanelli^{21,h}, R. Forty⁴⁴, V. Franco Lima⁵⁶, M. Frank⁴⁴, C. Frei⁴⁴, J. Fu^{23,q}, W. Funk⁴⁴, E. Gabriel⁵⁴, A. Gallas Torreira⁴³, D. Galli^{17,e}, S. Gallorini²⁵, S. Gambetta⁵⁴, Y. Gan³, M. Gandelman², P. Gandini²³, Y. Gao³, L.M. Garcia Martin⁷⁶, J. García Pardiñas⁴⁶, B. Garcia Plana⁴³, J. Garra Tico⁵¹, L. Garrido⁴², D. Gascon⁴², C. Gaspar⁴⁴, G. Gazzoni⁷, D. Gerick¹⁴, E. Gersabeck⁵⁸, M. Gersabeck⁵⁸, T. Gershon⁵², D. Gerstel⁸, Ph. Ghez⁶, V. Gibson⁵¹, O.G. Girard⁴⁵, P. Gironella Gironell⁴², L. Giubega³⁴, K. Gizdov⁵⁴, V.V. Gligorov¹⁰, C. Göbel⁶⁵,

D. Golubkov³⁶, A. Golutvin^{57,73}, A. Gomes^{1,a}, I.V. Gorelov³⁷, C. Gotti^{22,i}, E. Govorkova²⁹,
 J.P. Grabowski¹⁴, R. Graciani Diaz⁴², L.A. Granado Cardoso⁴⁴, E. Graugés⁴², E. Graverini⁴⁶,
 G. Graziani¹⁹, A. Grecu³⁴, R. Greim²⁹, P. Griffith²⁴, L. Grillo⁵⁸, L. Gruber⁴⁴,
 B.R. Gruberg Cazon⁵⁹, O. Grünberg⁷⁰, C. Gu³, E. Gushchin³⁸, A. Guth¹¹, Yu. Guz^{41,44},
 T. Gys⁴⁴, T. Hadavizadeh⁵⁹, C. Hadjivasilou⁷, G. Haefeli⁴⁵, C. Haen⁴⁴, S.C. Haines⁵¹,
 B. Hamilton⁶², X. Han¹⁴, T.H. Hancock⁵⁹, S. Hansmann-Menzemer¹⁴, N. Harnew⁵⁹,
 T. Harrison⁵⁶, C. Hasse⁴⁴, M. Hatch⁴⁴, J. He⁴, M. Hecker⁵⁷, K. Heinicke¹², A. Heister¹²,
 K. Hennessy⁵⁶, L. Henry⁷⁶, M. Heß⁷⁰, J. Heuel¹¹, A. Hicheur⁶⁴, R. Hidalgo Charman⁵⁸,
 D. Hill⁵⁹, M. Hilton⁵⁸, P.H. Hopchev⁴⁵, J. Hu¹⁴, W. Hu⁶⁸, W. Huang⁴, Z.C. Huard⁶¹,
 W. Hulsbergen²⁹, T. Humair⁵⁷, M. Hushchyn⁷⁴, D. Hutchcroft⁵⁶, D. Hynds²⁹, P. Ibis¹²,
 M. Idzik³², P. Ilten⁴⁹, A. Inglessi³⁵, A. Inyakin⁴¹, K. Ivshin³⁵, R. Jacobsson⁴⁴, S. Jakobsen⁴⁴,
 J. Jalocha⁵⁹, E. Jans²⁹, B.K. Jashal⁷⁶, A. Jawahery⁶², F. Jiang³, M. John⁵⁹, D. Johnson⁴⁴,
 C.R. Jones⁵¹, C. Joram⁴⁴, B. Jost⁴⁴, N. Jurik⁵⁹, S. Kandybei⁴⁷, M. Karacson⁴⁴, J.M. Kariuki⁵⁰,
 S. Karodia⁵⁵, N. Kazeev⁷⁴, M. Kecke¹⁴, F. Keizer⁵¹, M. Kelsey⁶³, M. Kenzie⁵¹, T. Ketel³⁰,
 E. Khairullin³⁹, B. Khanji⁴⁴, C. Khurewathanakul⁴⁵, K.E. Kim⁶³, T. Kirn¹¹, V.S. Kirsebom⁴⁵,
 S. Klaver²⁰, K. Klimaszewski³³, T. Klimkovich¹³, S. Kolliiev⁴⁸, M. Kolpin¹⁴, R. Kopečna¹⁴,
 P. Koppenburg²⁹, I. Kostiuk^{29,48}, S. Kotriakhova³⁵, M. Kozeiha⁷, L. Kravchuk³⁸, M. Kreps⁵²,
 F. Kress⁵⁷, P. Krokovny^{40,x}, W. Krupa³², W. Krzemien³³, W. Kucewicz^{31,l}, M. Kucharczyk³¹,
 V. Kudryavtsev^{40,x}, A.K. Kuonen⁴⁵, T. Kvaratskheliya^{36,44}, D. Lacarrere⁴⁴, G. Lafferty⁵⁸,
 A. Lai²⁴, D. Lancierini⁴⁶, G. Lanfranchi²⁰, C. Langenbruch¹¹, T. Latham⁵², C. Lazzeroni⁴⁹,
 R. Le Gac⁸, R. Lefèvre⁷, A. Leflat³⁷, F. Lemaître⁴⁴, O. Leroy⁸, T. Lesiak³¹, B. Leverington¹⁴,
 P.-R. Li^{4,ab}, Y. Li⁵, Z. Li⁶³, X. Liang⁶³, T. Likhomanenko⁷², R. Lindner⁴⁴, F. Lionetto⁴⁶,
 V. Lisovskyi⁹, G. Liu⁶⁶, X. Liu³, D. Loh⁵², A. Loi²⁴, I. Longstaff⁵⁵, J.H. Lopes², G. Loustau⁴⁶,
 G.H. Lovell⁵¹, D. Lucchesi^{25,o}, M. Lucio Martinez⁴³, Y. Luo³, A. Lupato²⁵, E. Luppi^{18,g},
 O. Lupton⁴⁴, A. Lusiani²⁶, X. Lyu⁴, F. Machefert⁹, F. Maciuc³⁴, V. Macko⁴⁵, P. Mackowiak¹²,
 S. Maddrell-Mander⁵⁰, O. Maev^{35,44}, K. Maguire⁵⁸, D. Maisuzenko³⁵, M.W. Majewski³²,
 S. Malde⁵⁹, B. Malecki⁴⁴, A. Malinin⁷², T. Maltsev^{40,x}, H. Malygina¹⁴, G. Manca^{24,f},
 G. Mancinelli⁸, D. Marangotto^{23,q}, J. Maratas^{7,w}, J.F. Marchand⁶, U. Marconi¹⁷,
 C. Marin Benito⁹, M. Marinangeli⁴⁵, P. Marino⁴⁵, J. Marks¹⁴, P.J. Marshall⁵⁶, G. Martellotti²⁸,
 M. Martinelli⁴⁴, D. Martinez Santos⁴³, F. Martinez Vidal⁷⁶, A. Massafferri¹, M. Materok¹¹,
 R. Matev⁴⁴, A. Mathad⁵², Z. Mathe⁴⁴, C. Matteuzzi²², K.R. Mattioli⁷⁷, A. Mauri⁴⁶,
 E. Maurice^{9,b}, B. Maurin⁴⁵, M. McCann^{57,44}, A. McNab⁵⁸, R. McNulty¹⁵, J.V. Mead⁵⁶,
 B. Meadows⁶¹, C. Meaux⁸, N. Meinert⁷⁰, D. Melnychuk³³, M. Merk²⁹, A. Merli^{23,q},
 E. Michielin²⁵, D.A. Milanese⁶⁹, E. Millard⁵², M.-N. Minard⁶, L. Minzoni^{18,g}, D.S. Mitzel¹⁴,
 A. Mödden¹², A. Mogini¹⁰, R.D. Moise⁵⁷, T. Mombächer¹², I.A. Monroy⁶⁹, S. Monteil⁷,
 M. Morandin²⁵, G. Morello²⁰, M.J. Morello^{26,t}, O. Morgunova⁷², J. Moron³², A.B. Morris⁸,
 R. Mountain⁶³, F. Muheim⁵⁴, M. Mukherjee⁶⁸, M. Mulder²⁹, D. Müller⁴⁴, J. Müller¹²,
 K. Müller⁴⁶, V. Müller¹², C.H. Murphy⁵⁹, D. Murray⁵⁸, P. Naik⁵⁰, T. Nakada⁴⁵,
 R. Nandakumar⁵³, A. Nandi⁵⁹, T. Nanut⁴⁵, I. Nasteva², M. Needham⁵⁴, N. Neri^{23,q},
 S. Neubert¹⁴, N. Neufeld⁴⁴, R. Newcombe⁵⁷, T.D. Nguyen⁴⁵, C. Nguyen-Mau^{45,n}, S. Nieswand¹¹,
 R. Niet¹², N. Nikitin³⁷, A. Nogay⁷², N.S. Nolte⁴⁴, A. Oblakowska-Mucha³², V. Obraztsov⁴¹,
 S. Ogilvy⁵⁵, D.P. O'Hanlon¹⁷, R. Oldeman^{24,f}, C.J.G. Onderwater⁷¹, A. Ossowska³¹,
 J.M. Otalora Goicochea², T. Ovsiannikova³⁶, P. Owen⁴⁶, A. Oyanguren⁷⁶, P.R. Pais⁴⁵,
 T. Pajero^{26,t}, A. Palano¹⁶, M. Palutan²⁰, G. Panshin⁷⁵, A. Papanestis⁵³, M. Pappagallo⁵⁴,
 L.L. Pappalardo^{18,g}, W. Parker⁶², C. Parkes^{58,44}, G. Passaleva^{19,44}, A. Pastore¹⁶, M. Patel⁵⁷,
 C. Patrignani^{17,e}, A. Pearce⁴⁴, A. Pellegrino²⁹, G. Penso²⁸, M. Pepe Altarelli⁴⁴, S. Perazzini⁴⁴,
 D. Pereima³⁶, P. Perret⁷, L. Pescatore⁴⁵, K. Petridis⁵⁰, A. Petrolini^{21,h}, A. Petrov⁷²,
 S. Petrucci⁵⁴, M. Petruzzio^{23,q}, B. Pietrzyk⁶, G. Pietrzyk⁴⁵, M. Pikiés³¹, M. Pili⁵⁹, D. Pinci²⁸,
 J. Pinzino⁴⁴, F. Pisani⁴⁴, A. Piucci¹⁴, V. Placinta³⁴, S. Playfer⁵⁴, J. Plews⁴⁹, M. Plo Casasus⁴³,
 F. Polci¹⁰, M. Poli Lener²⁰, A. Poluektov⁸, N. Polukhina^{73,c}, I. Polyakov⁶³, E. Polycarpo²,

G.J. Pomery⁵⁰, S. Ponce⁴⁴, A. Popov⁴¹, D. Popov^{49,13}, S. Poslavskii⁴¹, E. Price⁵⁰,
J. Prisciandaro⁴³, C. Prouve⁴³, V. Pugatch⁴⁸, A. Puig Navarro⁴⁶, H. Pullen⁵⁹, G. Punzi^{26,p},
W. Qian⁴, J. Qin⁴, R. Quagliani¹⁰, B. Quintana⁷, N.V. Raab¹⁵, B. Rachwal³²,
J.H. Rademacker⁵⁰, M. Rama²⁶, M. Ramos Pernas⁴³, M.S. Rangel², F. Ratnikov^{39,74},
G. Raven³⁰, M. Ravonel Salzgeber⁴⁴, M. Reboud⁶, F. Redi⁴⁵, S. Reichert¹², F. Reiss¹⁰,
C. Remon Alepuz⁷⁶, Z. Ren³, V. Renaudin⁵⁹, S. Ricciardi⁵³, S. Richards⁵⁰, K. Rinnert⁵⁶,
P. Robbe⁹, A. Robert¹⁰, A.B. Rodrigues⁴⁵, E. Rodrigues⁶¹, J.A. Rodriguez Lopez⁶⁹,
M. Roehrken⁴⁴, S. Roiser⁴⁴, A. Rollings⁵⁹, V. Romanovskiy⁴¹, A. Romero Vidal⁴³, J.D. Roth⁷⁷,
M. Rotondo²⁰, M.S. Rudolph⁶³, T. Ruf⁴⁴, J. Ruiz Vidal⁷⁶, J.J. Saborido Silva⁴³, N. Sagidova³⁵,
B. Saitta^{24,f}, V. Salustino Guimaraes⁶⁵, C. Sanchez Gras²⁹, C. Sanchez Mayordomo⁷⁶,
B. Sanmartin Sedes⁴³, R. Santacesaria²⁸, C. Santamarina Rios⁴³, M. Santimaria^{20,44},
E. Santovetti^{27,j}, G. Sarpis⁵⁸, A. Sarti^{20,k}, C. Satriano^{28,s}, A. Satta²⁷, M. Saur⁴, D. Savrina^{36,37},
S. Schael¹¹, M. Schellenberg¹², M. Schiller⁵⁵, H. Schindler⁴⁴, M. Schmelling¹³, T. Schmelzer¹²,
B. Schmidt⁴⁴, O. Schneider⁴⁵, A. Schopper⁴⁴, H.F. Schreiner⁶¹, M. Schubiger⁴⁵, S. Schulte⁴⁵,
M.H. Schune⁹, R. Schwemmer⁴⁴, B. Sciascia²⁰, A. Sciubba^{28,k}, A. Semennikov³⁶,
E.S. Sepulveda¹⁰, A. Sergi⁴⁹, N. Serra⁴⁶, J. Serrano⁸, L. Sestini²⁵, A. Seuthe¹², P. Seyfert⁴⁴,
M. Shapkin⁴¹, T. Shears⁵⁶, L. Shekhtman^{40,x}, V. Shevchenko⁷², E. Shmanin⁷³, B.G. Siddi¹⁸,
R. Silva Coutinho⁴⁶, L. Silva de Oliveira², G. Simi^{25,o}, S. Simone^{16,d}, I. Skiba¹⁸, N. Skidmore¹⁴,
T. Skwarnicki⁶³, M.W. Slater⁴⁹, J.G. Smeaton⁵¹, E. Smith¹¹, I.T. Smith⁵⁴, M. Smith⁵⁷,
M. Soares¹⁷, I. Soares Lavra¹, M.D. Sokoloff⁶¹, F.J.P. Soler⁵⁵, B. Souza De Paula², B. Spaan¹²,
E. Spadaro Norella^{23,q}, P. Spradlin⁵⁵, F. Stagni⁴⁴, M. Stahl¹⁴, S. Stahl⁴⁴, P. Stefko⁴⁵,
S. Stefkova⁵⁷, O. Steinkamp⁴⁶, S. Stemmler¹⁴, O. Stenyakin⁴¹, M. Stepanova³⁵, H. Stevens¹²,
A. Stocchi⁹, S. Stone⁶³, B. Storaci⁴⁶, S. Stracka²⁶, M.E. Stramaglia⁴⁵, M. Straticiu³⁴,
U. Straumann⁴⁶, S. Strovkov⁷⁵, J. Sun³, L. Sun⁶⁷, Y. Sun⁶², K. Swientek³², A. Szabelski³³,
T. Szumlak³², M. Szymanski⁴, Z. Tang³, T. Tekampe¹², G. Tellarini¹⁸, F. Teubert⁴⁴,
E. Thomas⁴⁴, M.J. Tilley⁵⁷, V. Tisserand⁷, S. T'Jampens⁶, M. Tobin³², S. Tolk⁴⁴,
L. Tomassetti^{18,g}, D. Tonelli²⁶, D.Y. Tou¹⁰, R. Tourinho Jadallah Aoude¹, E. Tournefier⁶,
M. Traill⁵⁵, M.T. Tran⁴⁵, A. Trisovic⁵¹, A. Tsaregorodtsev⁸, G. Tuci^{26,p}, A. Tully⁵¹,
N. Tuning^{29,44}, A. Ukleja³³, A. Usachov⁹, A. Ustyuzhanin^{39,74}, U. Uwer¹⁴, A. Vagner⁷⁵,
V. Vagnoni¹⁷, A. Valassi⁴⁴, S. Valat⁴⁴, G. Valenti¹⁷, M. van Beuzekom²⁹, E. van Herwijnen⁴⁴,
J. van Tilburg²⁹, M. van Veghel²⁹, R. Vazquez Gomez⁴⁴, P. Vazquez Regueiro⁴³,
C. Vázquez Sierra²⁹, S. Vecchi¹⁸, J.J. Velthuis⁵⁰, M. Veltri^{19,r}, A. Venkateswaran⁶³, M. Vernet⁷,
M. Veronesi²⁹, M. Vesterinen⁵², J.V. Viana Barbosa⁴⁴, D. Vieira⁴, M. Vieites Diaz⁴³,
H. Viemann⁷⁰, X. Vilasis-Cardona^{42,m}, A. Vitkovskiy²⁹, M. Vitti⁵¹, V. Volkov³⁷, A. Vollhardt⁴⁶,
D. Vom Bruch¹⁰, B. Voneki⁴⁴, A. Vorobyev³⁵, V. Vorobyev^{40,x}, N. Voropaev³⁵, R. Waldi⁷⁰,
J. Walsh²⁶, J. Wang⁵, M. Wang³, Y. Wang⁶⁸, Z. Wang⁴⁶, D.R. Ward⁵¹, H.M. Wark⁵⁶,
N.K. Watson⁴⁹, D. Websdale⁵⁷, A. Weiden⁴⁶, C. Weisser⁶⁰, M. Whitehead¹¹, G. Wilkinson⁵⁹,
M. Wilkinson⁶³, I. Williams⁵¹, M. Williams⁶⁰, M.R.J. Williams⁵⁸, T. Williams⁴⁹, F.F. Wilson⁵³,
M. Winn⁹, W. Wislicki³³, M. Witek³¹, G. Wormser⁹, S.A. Wotton⁵¹, K. Wyllie⁴⁴, D. Xiao⁶⁸,
Y. Xie⁶⁸, A. Xu³, M. Xu⁶⁸, Q. Xu⁴, Z. Xu⁶, Z. Xu³, Z. Yang³, Z. Yang⁶², Y. Yao⁶³,
L.E. Yeomans⁵⁶, H. Yin⁶⁸, J. Yu^{68,aa}, X. Yuan⁶³, O. Yushchenko⁴¹, K.A. Zarebski⁴⁹,
M. Zavertyaev^{13,c}, D. Zhang⁶⁸, L. Zhang³, W.C. Zhang^{3,z}, Y. Zhang⁴⁴, A. Zhelezov¹⁴,
Y. Zheng⁴, X. Zhu³, V. Zhukov^{11,37}, J.B. Zonneveld⁵⁴, S. Zucchelli^{17,e}.

¹Centro Brasileiro de Pesquisas Físicas (CBPF), Rio de Janeiro, Brazil

²Universidade Federal do Rio de Janeiro (UFRJ), Rio de Janeiro, Brazil

³Center for High Energy Physics, Tsinghua University, Beijing, China

⁴University of Chinese Academy of Sciences, Beijing, China

⁵Institute Of High Energy Physics (ihep), Beijing, China

⁶Univ. Grenoble Alpes, Univ. Savoie Mont Blanc, CNRS, IN2P3-LAPP, Annecy, France

⁷Université Clermont Auvergne, CNRS/IN2P3, LPC, Clermont-Ferrand, France

- ⁸ Aix Marseille Univ, CNRS/IN2P3, CPPM, Marseille, France
- ⁹ LAL, Univ. Paris-Sud, CNRS/IN2P3, Université Paris-Saclay, Orsay, France
- ¹⁰ LPNHE, Sorbonne Université, Paris Diderot Sorbonne Paris Cité, CNRS/IN2P3, Paris, France
- ¹¹ I. Physikalisches Institut, RWTH Aachen University, Aachen, Germany
- ¹² Fakultät Physik, Technische Universität Dortmund, Dortmund, Germany
- ¹³ Max-Planck-Institut für Kernphysik (MPIK), Heidelberg, Germany
- ¹⁴ Physikalisches Institut, Ruprecht-Karls-Universität Heidelberg, Heidelberg, Germany
- ¹⁵ School of Physics, University College Dublin, Dublin, Ireland
- ¹⁶ INFN Sezione di Bari, Bari, Italy
- ¹⁷ INFN Sezione di Bologna, Bologna, Italy
- ¹⁸ INFN Sezione di Ferrara, Ferrara, Italy
- ¹⁹ INFN Sezione di Firenze, Firenze, Italy
- ²⁰ INFN Laboratori Nazionali di Frascati, Frascati, Italy
- ²¹ INFN Sezione di Genova, Genova, Italy
- ²² INFN Sezione di Milano-Bicocca, Milano, Italy
- ²³ INFN Sezione di Milano, Milano, Italy
- ²⁴ INFN Sezione di Cagliari, Monserrato, Italy
- ²⁵ INFN Sezione di Padova, Padova, Italy
- ²⁶ INFN Sezione di Pisa, Pisa, Italy
- ²⁷ INFN Sezione di Roma Tor Vergata, Roma, Italy
- ²⁸ INFN Sezione di Roma La Sapienza, Roma, Italy
- ²⁹ Nikhef National Institute for Subatomic Physics, Amsterdam, Netherlands
- ³⁰ Nikhef National Institute for Subatomic Physics and VU University Amsterdam, Amsterdam, Netherlands
- ³¹ Henryk Niewodniczanski Institute of Nuclear Physics Polish Academy of Sciences, Kraków, Poland
- ³² AGH - University of Science and Technology, Faculty of Physics and Applied Computer Science, Kraków, Poland
- ³³ National Center for Nuclear Research (NCBJ), Warsaw, Poland
- ³⁴ Horia Hulubei National Institute of Physics and Nuclear Engineering, Bucharest-Magurele, Romania
- ³⁵ Petersburg Nuclear Physics Institute (PNPI), Gatchina, Russia
- ³⁶ Institute of Theoretical and Experimental Physics (ITEP), Moscow, Russia
- ³⁷ Institute of Nuclear Physics, Moscow State University (SINP MSU), Moscow, Russia
- ³⁸ Institute for Nuclear Research of the Russian Academy of Sciences (INR RAS), Moscow, Russia
- ³⁹ Yandex School of Data Analysis, Moscow, Russia
- ⁴⁰ Budker Institute of Nuclear Physics (SB RAS), Novosibirsk, Russia
- ⁴¹ Institute for High Energy Physics (IHEP), Protvino, Russia
- ⁴² ICCUB, Universitat de Barcelona, Barcelona, Spain
- ⁴³ Instituto Galego de Física de Altas Enerxías (IGFAE), Universidade de Santiago de Compostela, Santiago de Compostela, Spain
- ⁴⁴ European Organization for Nuclear Research (CERN), Geneva, Switzerland
- ⁴⁵ Institute of Physics, Ecole Polytechnique Fédérale de Lausanne (EPFL), Lausanne, Switzerland
- ⁴⁶ Physik-Institut, Universität Zürich, Zürich, Switzerland
- ⁴⁷ NSC Kharkiv Institute of Physics and Technology (NSC KIPT), Kharkiv, Ukraine
- ⁴⁸ Institute for Nuclear Research of the National Academy of Sciences (KINR), Kyiv, Ukraine
- ⁴⁹ University of Birmingham, Birmingham, United Kingdom
- ⁵⁰ H.H. Wills Physics Laboratory, University of Bristol, Bristol, United Kingdom
- ⁵¹ Cavendish Laboratory, University of Cambridge, Cambridge, United Kingdom
- ⁵² Department of Physics, University of Warwick, Coventry, United Kingdom
- ⁵³ STFC Rutherford Appleton Laboratory, Didcot, United Kingdom
- ⁵⁴ School of Physics and Astronomy, University of Edinburgh, Edinburgh, United Kingdom
- ⁵⁵ School of Physics and Astronomy, University of Glasgow, Glasgow, United Kingdom
- ⁵⁶ Oliver Lodge Laboratory, University of Liverpool, Liverpool, United Kingdom
- ⁵⁷ Imperial College London, London, United Kingdom
- ⁵⁸ School of Physics and Astronomy, University of Manchester, Manchester, United Kingdom
- ⁵⁹ Department of Physics, University of Oxford, Oxford, United Kingdom
- ⁶⁰ Massachusetts Institute of Technology, Cambridge, MA, United States

- ⁶¹ *University of Cincinnati, Cincinnati, OH, United States*
⁶² *University of Maryland, College Park, MD, United States*
⁶³ *Syracuse University, Syracuse, NY, United States*
⁶⁴ *Laboratory of Mathematical and Subatomic Physics, Constantine, Algeria, associated to ²*
⁶⁵ *Pontifícia Universidade Católica do Rio de Janeiro (PUC-Rio), Rio de Janeiro, Brazil, associated to ²*
⁶⁶ *South China Normal University, Guangzhou, China, associated to ³*
⁶⁷ *School of Physics and Technology, Wuhan University, Wuhan, China, associated to ³*
⁶⁸ *Institute of Particle Physics, Central China Normal University, Wuhan, Hubei, China, associated to ³*
⁶⁹ *Departamento de Física, Universidad Nacional de Colombia, Bogota, Colombia, associated to ¹⁰*
⁷⁰ *Institut für Physik, Universität Rostock, Rostock, Germany, associated to ¹⁴*
⁷¹ *Van Swinderen Institute, University of Groningen, Groningen, Netherlands, associated to ²⁹*
⁷² *National Research Centre Kurchatov Institute, Moscow, Russia, associated to ³⁶*
⁷³ *National University of Science and Technology "MISIS", Moscow, Russia, associated to ³⁶*
⁷⁴ *National Research University Higher School of Economics, Moscow, Russia, associated to ³⁹*
⁷⁵ *National Research Tomsk Polytechnic University, Tomsk, Russia, associated to ³⁶*
⁷⁶ *Instituto de Física Corpuscular, Centro Mixto Universidad de Valencia - CSIC, Valencia, Spain, associated to ⁴²*
⁷⁷ *University of Michigan, Ann Arbor, United States, associated to ⁶³*
⁷⁸ *Los Alamos National Laboratory (LANL), Los Alamos, United States, associated to ⁶³*

- ^a *Universidade Federal do Triângulo Mineiro (UFMT), Uberaba-MG, Brazil*
^b *Laboratoire Leprince-Ringuet, Palaiseau, France*
^c *P.N. Lebedev Physical Institute, Russian Academy of Science (LPI RAS), Moscow, Russia*
^d *Università di Bari, Bari, Italy*
^e *Università di Bologna, Bologna, Italy*
^f *Università di Cagliari, Cagliari, Italy*
^g *Università di Ferrara, Ferrara, Italy*
^h *Università di Genova, Genova, Italy*
ⁱ *Università di Milano Bicocca, Milano, Italy*
^j *Università di Roma Tor Vergata, Roma, Italy*
^k *Università di Roma La Sapienza, Roma, Italy*
^l *AGH - University of Science and Technology, Faculty of Computer Science, Electronics and Telecommunications, Kraków, Poland*
^m *LIFAEELS, La Salle, Universitat Ramon Llull, Barcelona, Spain*
ⁿ *Hanoi University of Science, Hanoi, Vietnam*
^o *Università di Padova, Padova, Italy*
^p *Università di Pisa, Pisa, Italy*
^q *Università degli Studi di Milano, Milano, Italy*
^r *Università di Urbino, Urbino, Italy*
^s *Università della Basilicata, Potenza, Italy*
^t *Scuola Normale Superiore, Pisa, Italy*
^u *Università di Modena e Reggio Emilia, Modena, Italy*
^v *H.H. Wills Physics Laboratory, University of Bristol, Bristol, United Kingdom*
^w *MSU - Iligan Institute of Technology (MSU-IIT), Iligan, Philippines*
^x *Novosibirsk State University, Novosibirsk, Russia*
^y *Sezione INFN di Trieste, Trieste, Italy*
^z *School of Physics and Information Technology, Shaanxi Normal University (SNNU), Xi'an, China*
^{aa} *Physics and Micro Electronic College, Hunan University, Changsha City, China*
^{ab} *Lanzhou University, Lanzhou, China*

† *Deceased*